Carbohydrate Polymer Technologies and Applications 6 (2023) 100365

Contents lists available at ScienceDirect

Carbohydrate Polymer Technologies and Applications

journal homepage: www.sciencedirect.com/journal/carbohydrate-polymer-technologies-and-applications

Silver phosphate–bacterial cellulose nanocomposites as visible light photocatalyst for wastewater purification

Amruth Kaitheri [a], Sanosh Kunjalukkal Padmanabhan [a,*], Sudipto Pal [a], Mariangela Stoppa [a,b], Antonio Licciulli [a,c]

[a] Department of Engineering for Innovation (DII), University of Salento, Lecce 73100, Italy
[b] BioFaber Srl, Via Luigi di Savoia, 19, Mesagne 72023, Italy
[c] Institute of Nanotechnology, CNR Nanotec, Consiglio Nazionale Delle Ricerche, Via Monteroni, Lecce 73100, Italy

ARTICLE INFO

Keywords:
Silver phosphate
Bacterial cellulose: Visible light photocatalysis
Textile dyes

ABSTRACT

Silver phosphate (Ag_3PO_4) nanoparticles were deposited on bacterial cellulose (BC) nanofibrils as an eco-friendly, efficient, and reusable visible light active photocatalyst. BC–Ag_3PO_4 nanocomposites (BCAgP) with different BC/Ag_3PO_4 weight ratios were prepared by solution-precipitation method. The nanocomposites were characterized by UV-Visible diffuse reflection spectroscopy, XRD, FTIR, BET, and FESEM. Highly crystalline Ag_3PO_4 nanoparticles were well entrapped inside nano fibrillated BC matrix and eventually deposited along the fibers. Photocatalytic activity of the BCAgP nanocomposites were investigated by dye degradation experiments under solar light. The composite with BC: Ag_3PO_4 weight ratio of 1:4 (BCAgP14) showed the highest photocatalytic efficiency compared to other weight ratios and pure Ag_3PO_4. The sample also shows good photocatalytic activity even after 4 runs indicating its photostability. Higher photocatalytic efficiency of BCAgP14 nanocomposite was explained due to optimum Ag_3PO_4 loading and higher visible light absorption capacity. Bacterial cellulose is supposed to improve the photocatalytic activity of silver phosphate by promoting the adsorption of dyes and extending the charge recombination time under visible light of Ag_3PO_4 photocatalyst.

1. Introduction

Environmental pollution and contamination of water are today a major concern (Nash, 2008). Textile industries have been identified as the major contributors to water pollution since wastewater from textile processing contains hazardous chemicals, dyes, heavy metals, and other pollutants that can contaminate water sources such as rivers and lakes (Srebrenkoska, Zhezhova, Risteski, & Golomeova, 2014). Studies show that photocatalysis is an effective method for the removal of harmful pollutants present in the air, waterbodies etc (Pal et al., 2023; Salim et al., 2019). TiO_2, ZnO, g-C_3N_4, WO_3, Fe_2O_3, CdS, ZnS, Ag_3PO_4 etc. are some of the most discussed photocatalysts (Bedia et al., 2019; Fu et al., 2018; Mishra & Chun, 2015; Szilágyi et al., 2012; Tian et al., 2012). Researchers are more interested in developing visible light photocatalysts as they can be activated by sunlight.

Silver (Ag) and its compounds have been extensively researched for their photocatalytic capabilities (Huang et al., 2020). Ag composites have a lot of potential characteristics for photocatalytic applications like their broad absorption in the visible region, plasmonic effects, etc. (Rahmawati et al., 2014). They can improve the efficiency and selectivity of the catalytic process (Liu et al., 2007). Among them, silver phosphate (Ag_3PO_4) is considered to be an excellent visible light active photocatalyst with a bandgap of about 2.4 eV, and compared to other metal-based photocatalysts, it exhibits strong photocatalytic activity, and can be synthesized in an ambient temperature (James Martin et al., 2015; Rahmawati et al., 2014). Silver phosphate is a cubic crystal where, PO_4 tetrahedra are coordinated with Ag cations. AgP has been investigated for a variety of applications, such as wastewater treatment, air purification, antibacterial activity etc (Chai et al., 2022). Studies prove that AgP can be effectively used to break down organic contaminants in water. Therefore, it can be considered as an effective photocatalytic material for water purification (Li et al., 2019; Tavker et al., 2020). Even though silver phosphate is considered as a superior photocatalyst, its stability and separation after reaction are still under question. There has been many attempts to increase the stability and performance of AgP as a photocatalyst by combining it with metal oxides like SnO_2, TiO_2,

* Corresponding author.
E-mail address: sanosh.padmanabhan@unisalento.it (S. Kunjalukkal Padmanabhan).

https://doi.org/10.1016/j.carpta.2023.100365

Available online 26 September 2023

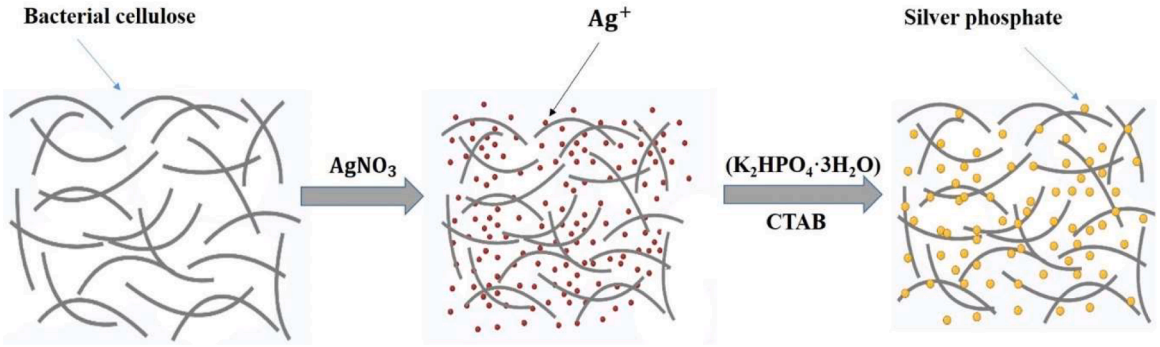

Fig. 1. Schematic illustration of bacterial cellulose – silver phosphate (BCAgP) composites.

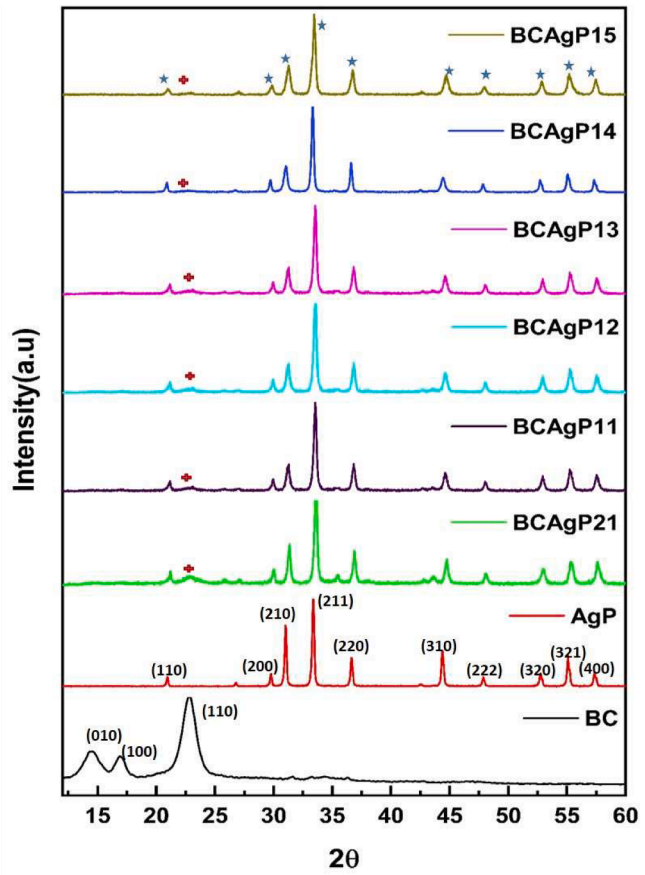

Fig. 2. The XRD patterns of pure silver phosphate, bacterial cellulose, and their composites with different BC/AgP weight ratios.

Table 1
BET specific surface area, the pore diameter, pore volume, and the crystallite size of BC, AgP and BCAgP composites.

Sample	BET surface area (m^2/g)	Mean pore diameter (nm)	Pore volume (cc/g)	Crystallite size (nm)
BC	**18.01**	**3.7**	**0.077**	**-**
AgP	**7.21**	**3.0**	**0.016**	**37.8**
BCAgP21	**10.78**	**3.7**	**0.050**	**18**
BCAgP11	**13.13**	**3.7**	**0.051**	**23.3**
BCAgP12	**13.22**	**3.6**	**0.045**	**25.6**
BCAgP13	**13.42**	**3.8**	**0.060**	**27.4**
BCAgP14	**14.27**	**3.8**	**0.068**	**30.9**
BCAgP15	**14.92**	**3.8**	**0.072**	**34.5**

Fe_3O_4, etc. and support materials like CNT, chitosan, diatomite, etc (Kamel, 2004; Lin et al., 2013; Rajwade et al., 2015; Rana et al., 2021; Yang et al., 2022). The main challenge of researchers is to develop a photocatalyst that is active in the visible range and eco-friendly at the same time.

Recent studies have revealed that cellulose supported semiconductors can be used as an efficient photocatalyst for water purification treatments (Rana et al., 2021). There have been some interesting reports regarding the utilization of cellulose extracted from various sources as a supporting material for different photocatalysts to aid its efficiency (Tavker et al., 2020; Yang et al., 2022). Its structure has a large number of electron-rich hydroxyl groups, which will improve the catalytic activity of the photocatalyst (Kamel, 2004; Tavker et al., 2020). Recently Tavker et al. (2020) has reported that cellulose extracted from food wastes can be used as a support material and they developed cellulose supported silver phosphate nano structures for the degradation of pollutants in water. In this regard, we tried to explore bacterial cellulose for making cellulose/silver phosphate nanocomposite photocatalysts. Bacterial cellulose is a nanofibril with a distinct structure and set of features that make it a valuable material for a variety of applications (Fu et al., 2013; Lin et al., 2013; Rajwade et al., 2015). It has unique qualities like high purity, biocompatibility, high porosity, high degree of crystallinity, non-toxic, high tensile strength flexibility etc (Dourado et al., 2017; Güzel & Akpınar, 2019; Krystynowicz et al., 2002). Its porous, structural, and biological properties are mostly utilized in wound dressings, tissue engineering, medical implants, artificial skin, food production, clothing and textiles etc (Güzel & Akpınar, 2019; Provin et al., 2021; Shi et al., 2014). As the world moves towards a sustainable and cleaner phase, bacterial cellulose has been highlighted as a novel nano-material with an extensive range of distinct properties, making it an excellent industrial alternative to conventional plant cellulose. We assume that these inherent properties of BC will make it an excellent green material network structure for incorporating different photocatalysts. To the best of our knowledge, the photocatalytic property of BC-silver phosphate composite has not been reported till date. In this paper, we studied the synthesis and characterization of visible light active bacterial cellulose-silver phosphate (BCAgP) nanocomposites and their application for wastewater treatment. The composites were analyzed by UV-visible spectrophotometry, SEM, XRD, BET, FTIR, and photocatalytic activity was evaluated by performing photodegradation of Rhodamine B (RhB) and Methylene blue (MB) dyes under visible light irradiation.

2. Experimental

2.1. Materials

Silver nitrate ($AgNO_3$) was obtained from J.T Baker, Potassium phosphate dibasic trihydrate ($HK_2O_4P.3H_2O$) was obtained from sigma Aldrich and CTAB (1-Hexadecyl) trimethylammonium bromide, 98 %

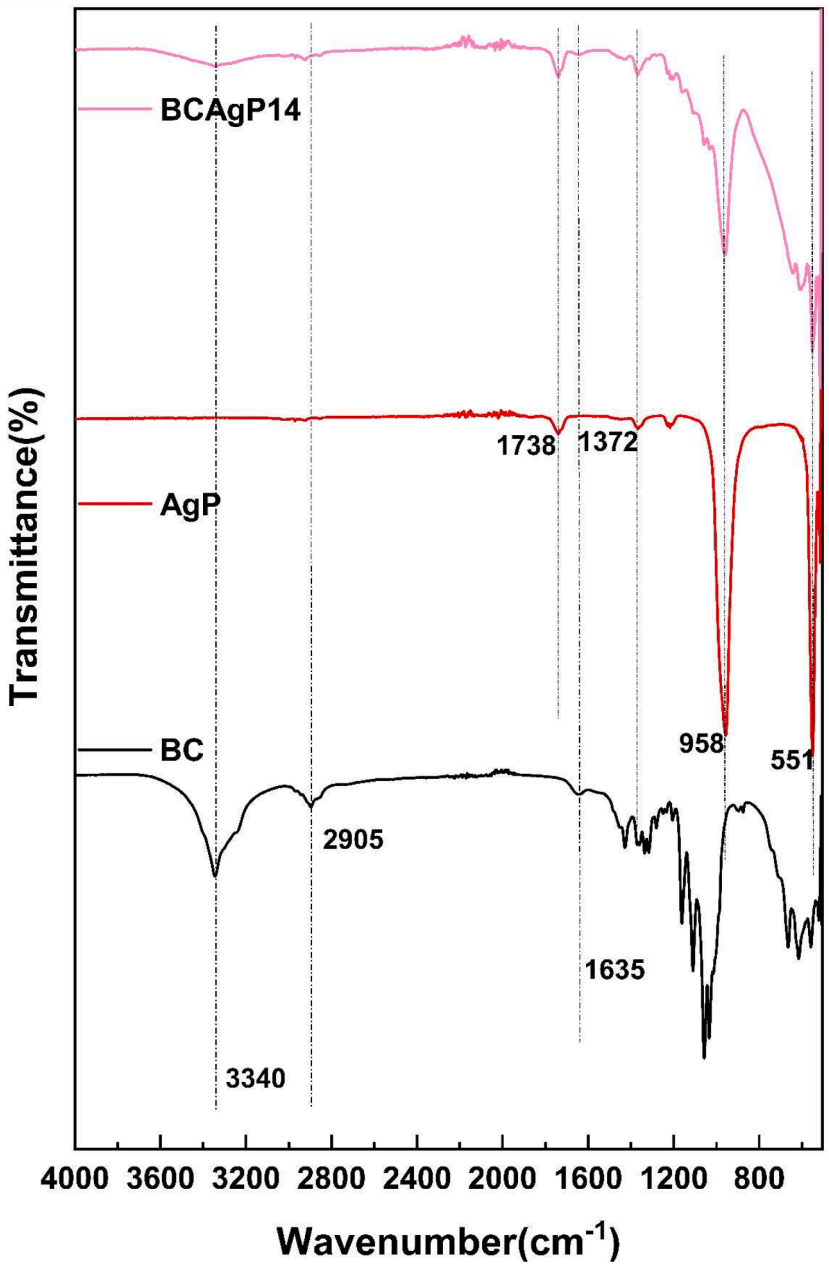

Fig. 3. The FTIR spectra of BC, AgP and BCAgP 14.

$(CH_3(CH_2)_{15}N(CH_3)_3Br)$ was obtained from Alfa aeser. Black tea bags (Sir Bolton Company), commercial sucrose, commercial vinegar and Kombucha tea were bought from a local market. Demineralized water was used throughout the synthesis process.

2.2. Synthesis of bacterial cellulose

Bacterial cellulose hydrogels were prepared from the kombucha strains by the fermentation of sweetened black tea with acetobacter strains according to our previous works (Kunjalukkal Padmanabhan et al., 2023; Pal et al., 2017). The culture medium was produced by adding sugar and tea bags to 1 liter of boiling water. The pH of the broth was adjusted to neutral by adding acetic acid to it. At last, the cellulose pellicles and liquid broth of the tea fungus were added to the cooled tea broth. The fermentation process was then carried out at room temperature for 15 days in a static culture condition. New pellicles of cellulose were grown on the surface of the broth, and they were washed with distilled water and boiled in 0.5 M NaOH solution for purification. The bacterial cellulose then obtained were fibrillated using a high-speed blender and centrifuged at 7000 rpm for 5 min to remove the excess water. Bacterial cellulose pulp for composite synthesis was made by fibrillating purified BC pieces using a high-speed blender and centrifuged at 7000 rpm for 5 min to remove the excess water. The sample was then dried and a pulp having 2wt. % of dry bacterial cellulose was obtained.

2.3. Synthesis of bacterial cellulose-silver phosphate nanocomposite

The synthesis of nano-sized bacterial cellulose-silver phosphate composite nanostructure was carried out by an *in-situ* approach. For making BCAgP composites, bacterial cellulose pulp was dispersed in distilled water by magnetic stirring. Silver nitrate was added to the cellulose dispersion and stirred overnight to let the Ag^+ ions to be adsorbed on the surface of the cellulose. An aqueous solution of

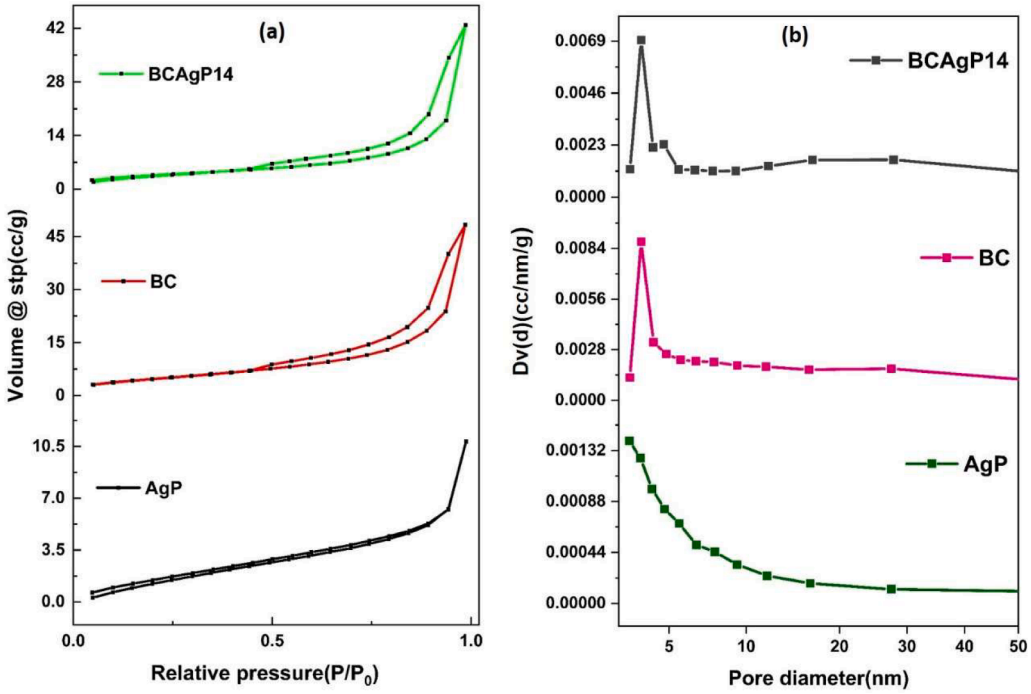

Fig. 4. N_2 sorption isotherms (a) and BJH pore size distribution (b) of AgP, BC and BCAgP14 samples.

dipotassium hydrogen phosphate ($K_2HPO_4{\cdot}3H_2O$) containing a definite amount of CTAB was added dropwise to Ag-BC suspension and a yellow precipitate was formed. The addition of CTAB was to reduce the size of the silver phosphate to a nanometric range (Tavker et al., 2020). The precipitate was centrifuged and washed with hot water, ethanol and dried at 70°C overnight to get dried composite powder samples. Different weight ratios of bacterial cellulose supported silver phosphate samples were prepared (2:1, 1:1, 1:2, 1:3, 1:4 and 1:5) namely BCAgP21, BCAgP11, BCAgP12, BCAgP13, BCAgP14 and BCAgP15 respectively and the samples were subjected to further analysis and characterization studies. Pure Ag3PO4 was produced by keeping the Ag/P molar ratio at 3:1 without adding BC pulp. A schematic representation of the synthesis of BCAgP composite is shown in Fig. 1.

2.4. Characterisation of BCAgP nanocomposites

The crystallographic structures of the samples were analyzed using an X-ray powder diffraction (XRD) using Rigaku Ultima diffractometer, with Cu Kα radiations generated at 40 kV and 20 mA. The morphology of pure silver phosphate (AgP), bacterial cellulose (BC), and bacterial cellulose/silver phosphate composites (BCAgP) were studied using an EVO-Zeiss (Jena, Germany) scanning electron microscope (SEM). The nitrogen adsorption/ desorption measurements were performed using NOVA 2200e (Quantachrome, Anton Paar USA Inc., Timber Ridge, VA, USA) apparatus at a temperature of −196 °C. The samples were degassed overnight at 90 °C. The multipoint Brunauer–Emmett–Teller (BET) technique was used to calculate the specific surface area (SSA) using adsorption data in the relative pressure range of 0.05–0.25 and the pore size distribution was calculated by Barrett-Joyner-Halenda (BJH) method using desorption isotherm. The UV-visible absorption spectra and diffuse reflectance spectra (DRS) were measured using an Agilent Carry 5000 UV-visible-NIR spectrophotometer (Agilent Technologies Inc., Santa Clara, CA, USA) in the wavelength range of 200–800 nm equipped with a standard PTFE 150 mm diameter integrating sphere. The Fourier transform infrared spectroscopy (FTIR) of the samples was recorded in attenuated total reflectance (ATR) mode with a Perkin Elmer Spectrum One spectrometer (Perkin Elmer, Waltham,) USA at a wavelength range of 500–4000 cm^{-1} with a resolution of 4 cm^{-1}.

2.5. Characterization of photocatalytic activity

Rhodamine B (RhB) and Methylene Blue (MB) were used as the model pollutant in dye degradation studies. The experimental setup consisted of a photocatalytic chamber equipped with 300W tungsten lamp (Sanolux, Radium Lampenwerk, Irradiance 41.4 W m^{-2} at 380–700 nm wavelength), a magnetic stirring system, and a vent to cool the system. The photocatalyst samples (1 g L^{-1}) were dispersed in 100 mL of RhB/MB aqueous solution (5 ppm) and stirred overnight in the dark to attain adsorption-desorption equilibrium. Then the suspensions were exposed to solar lamp irradiation and the samples were collected in a fixed time interval (5 min.) and subjected to centrifugation. The recyclability of the samples was tested for 4 runs under the same conditions. An Agilent Cary 5000 series UV-visible spectrophotometer was used to record the absorption spectra of the samples and to observe the photodecomposition of the dye solutions.

3. Results and discussions

The XRD spectra of BC, AgP, and their composites are shown in Fig. 2 The Crystalline peaks of BC and AgP are clearly visible in their XRD spectra. For AgP and the BCAgP composites, there are clear diffraction peaks at 20.9°, 29.7°, 30.9°, 33.2°, 36.5°, 44.3°, 47.8°, 52.7°, 55.1°, 61.7° and 64.5° with the corresponding miller indices (110), (200), (210), (211), (220), (310), (222), (320), (321), (400), and (411), which confirms the formation of silver phosphate in the BC matrix (Tavker et al., 2020). Pure BC shows strong and relatively broad diffraction peaks of nanosized crystalline cellulose whereas all these peaks are hardly visible in the case of the composite samples. The presence of silver phosphate in the composites may camouflage the crystalline structure of bacterial cellulose, resulting in the diminishing of BC peaks in the composites. The crystallite size of silver phosphate in the composite samples was calculated using the Scherer equation [(D=kλ/β cos θ); where D is the crystallite size, $k = 0.9$ for bcc, λ is the XRD wavelength which is 1.54 A°, β is the full width at the half maximum of the peak with the maximum intensity (211) and θ is obtained from the diffraction angle (2θ) corresponding to (211) peak] and are reported in Table 1. From the data (Table 1), it could be seen that the BCAgP composites with a higher

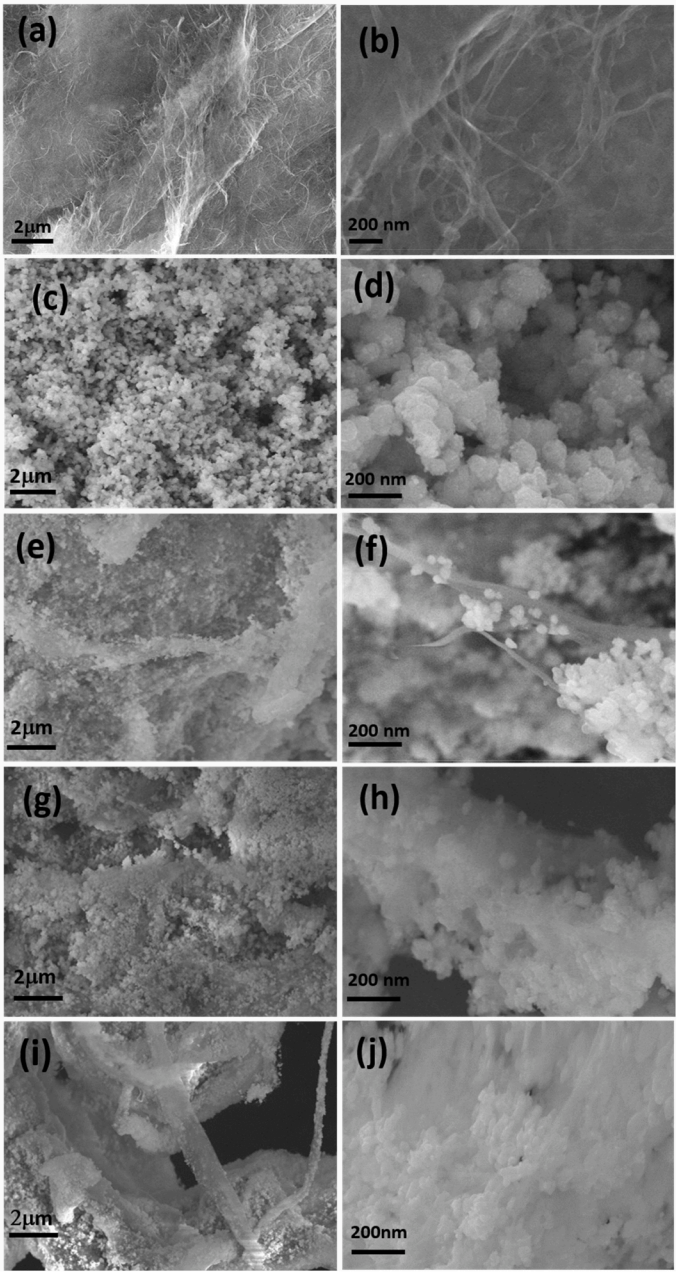

Fig. 5. FESEM images of bacterial cellulose (a, b), silver phosphate (c, d), BCAgP21 (e, f), BCAgP14 (g, h) and BCAgP15 (i, j).

percentage of silver phosphate have a larger crystallite size, and vice versa.

In Fig. 3 the FTIR spectra of BC, AgP and BCAgP14 are reported. A strong absorbance at 3340 cm^{-1}, 2905 and 1635 cm^{-1} was observed for pure BC due to the O-H stretching, C-H stretching and H-O-H bending vibration of absorbed water molecules respectively (Tavker et al., 2020). In the case of AgP, the flexural and asymmetric stretching vibrations of P-O are represented by the peaks at 552 cm^{-1} and 950 cm^{-1}, respectively, and the bending vibrations of H-O-H are represented by peaks at 1334 cm^{-1} and 1662 cm^{-135}. Representative peaks of both cellulose and silver phosphate are evident in the FTIR spectra of BCAgP14, which confirms the formation of bacterial cellulose–silver phosphate composite.

The textural properties of all samples were analyzed using N_2 adsorption/desorption method. In Fig. 4 the adsorption-desorption isotherm and pore size distribution of BC, AgP, and BCAgP14 samples are showed, and all three samples show a type (II) isotherm. In the case of pure AgP, the isotherm shows no volume uptake in the partial pressure region (0.45–0.9). The BET specific surface area, BJH pore size, and pore volume of all the samples were reported in Table 1. The specific surface area of BC and AgP was found to be 18 m^2/g and 7.2 m^2/g, respectively. Among all the six BCAgP composites BCAgP15 exhibited the highest specific surface area, pore diameter, and pore volume (19.9 m^2/g, 3.7 nm and 0.112 cc/g, respectively). All BCAgP composites showed a higher specific surface area than pure AgP, which indicates that cellulose support enhances the textural property of AgP in their composites. When we look into the trend of the specific surface area of the samples, it is observed that when the amount of silver phosphate increases the specific surface area also increases. This is possibly due to the controlled precipitation process of silver phosphate particles by the porous structure of cellulose. All samples showed the same pore diameter of about 3.7 nm whereas pore volume increased with an increase in the silver phosphate content in the composites.

The microstructural properties of bacterial cellulose (BC), silver

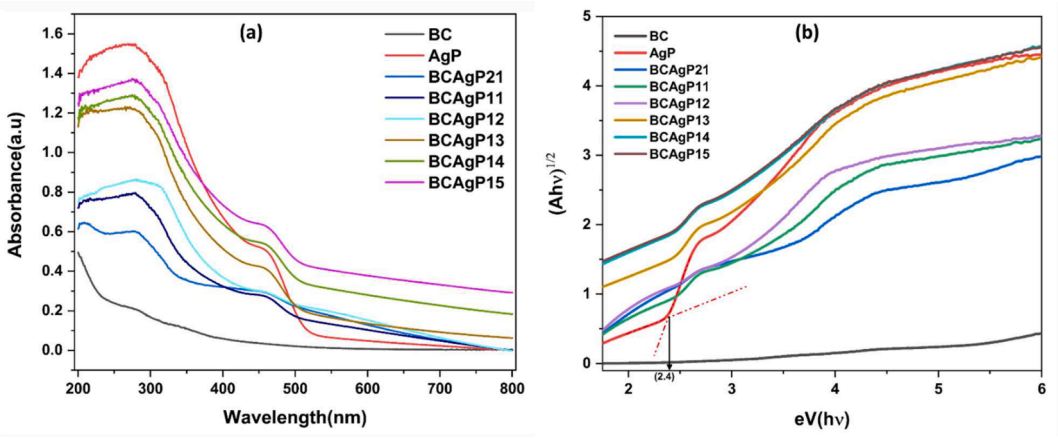

Fig. 6. (a) UV–visible absorption spectra of the pure AgP, BC, and the composites; (b) $(Ah\nu)^{1/2}$ against photon energy hν (eV) curve derived from the absorption spectra.

Table 2
The rate constant and energy bandgap of pure silver phosphate, bacterial cellulose, and their composites in 5ppm MB and RhB.

Sample name	Rate constant (k) in min^{-1}		Energy bandgap (eV)
	RhB	MB	
BC	0.002	0.016	-
AgP	0.05	0.1	2.40
BCAgP21	0.050	0.028	2.48
BCAgP11	0.087	0.064	2.47
BCAgP12	0.071	0.076	2.48
BCAgP13	0.159	0.101	2.45
BCAgP14	0.173	0.122	2.45
BCAgP15	0.135	0.091	2.48

phosphate (AgP) and their composites (BCAgP) were analyzed through Field Emission Scanning Electron Microscopy (FESEM). The SEM images of AgP, BC, and their composites with different magnifications are shown in Fig. 5. The nanofibrils of bacterial cellulose can be detected in the SEM images (Fig. 5a, b). The nano-fibrous structure of the BC was sustained even after mechanical fibrillation. The microstructure of pure AgP (Fig. 5c&d) consists of particles with spherical morphology with an average size of 100 nm. The SEM images of BCAgP composites are shown in Fig. 5e–j. It is evident from the SEM images that, with the increasing amount of silver phosphate, the cellulose network is densely packed with silver phosphate particles (Fig. 5h &j). In a higher magnification SEM image of BCAgP14 (Fig. 5f), it is clearly visible that the silver phosphate particles having a size around 60–70 nm are attached to the bacterial cellulose fiber. Thanks to CTAB, which acts as a capping agent to reduce the size of the silver phosphate particles to a nanometric scale (Tavker et al., 2020). In Fig. 5j, which represents BCAgP15, the amount of silver phosphate is five times more than that of bacterial cellulose, and thus a cluster of agglomerated silver phosphate particles which has a dimension in submicron range can be noticed around the bacterial cellulose fibers.

The UV-visible diffuse reflectance spectra of the pristine AgP and BCAgP composite samples are reported in Fig. 6. A distinct absorption in the 460–500 nm wavelength range is observed for pure Ag3PO4 with an absorption edge at around 517.6 nm (calculated from the Tauc's plot), which is in good agreement with the energy band gap of pure Ag3PO4 (~2.40 eV, estimated from DRS spectra, Table 2). The energy bandgap is calculated by plotting the square root of the product of photon energy (hν) and absorption coefficient (A) against the photon energy (hν). The intersection between the base and the absorption edge of each curve represents the bandgap energy of the corresponding samples. The equation $(Ah\nu)^{1/2}$ v/s hν is derived from Beer-Lambert's absorption law and the determination of energy bandgap was done by plotting $(Ah\nu)^{1/2}$ v/s hν (Fig. 6) in origin and the calculated energy bandgap values are listed in Table 2. As we can see, the bandgap values for composites are in good agreement with the visible light energy range (1.8 eV–3.1 eV), and the energy bandgaps of BCAgP composites are a bit higher than that of pure silver phosphate.

The photocatalytic activity of the samples was evaluated by the degradation of Rhodamine B (RhB) and Methylene Blue (MB) dyes under

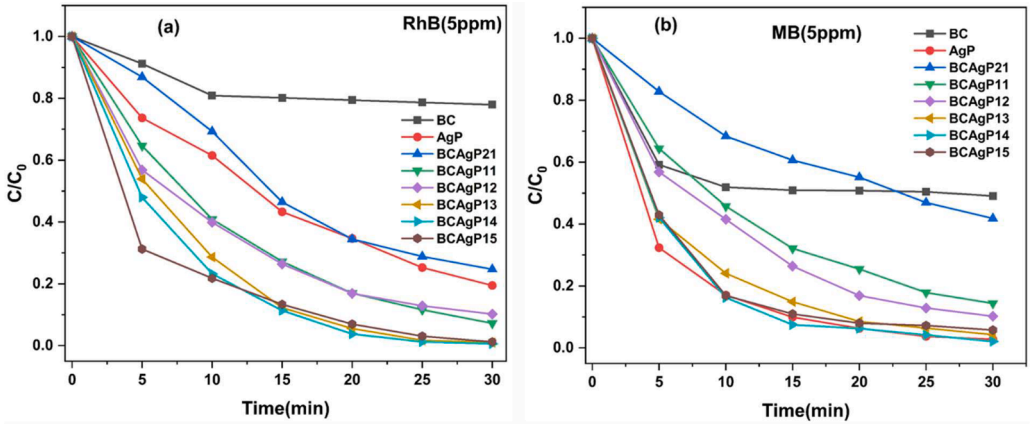

Fig. 7. (a) C/C_0 v/s Irradiation time of 5 ppm RhB and (b) C/C_0 v/s Irradiation time of 5 ppm MB in pure silver phosphate, bacterial cellulose and their composites respectively.

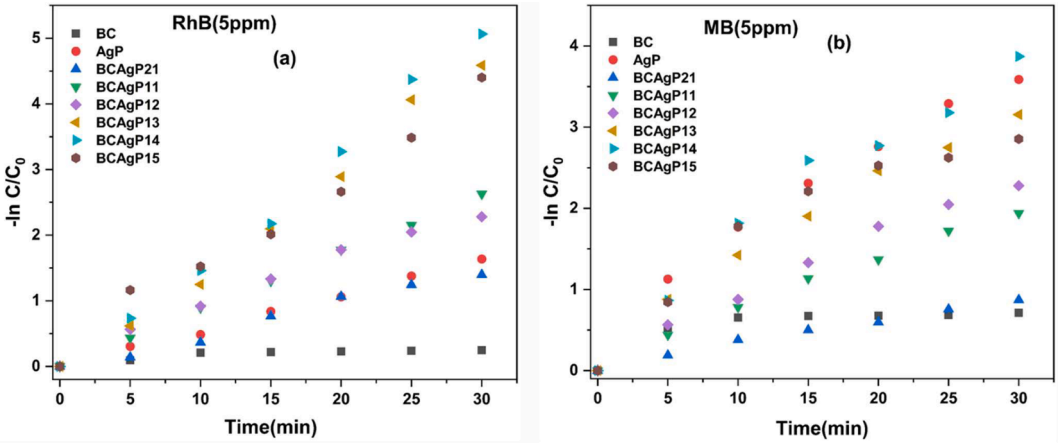

Fig. 8. ln C/C_0 v/s irradiation time of 5ppm RhB (a) and MB (b) in pure silver phosphate, bacterial cellulose and their composites.

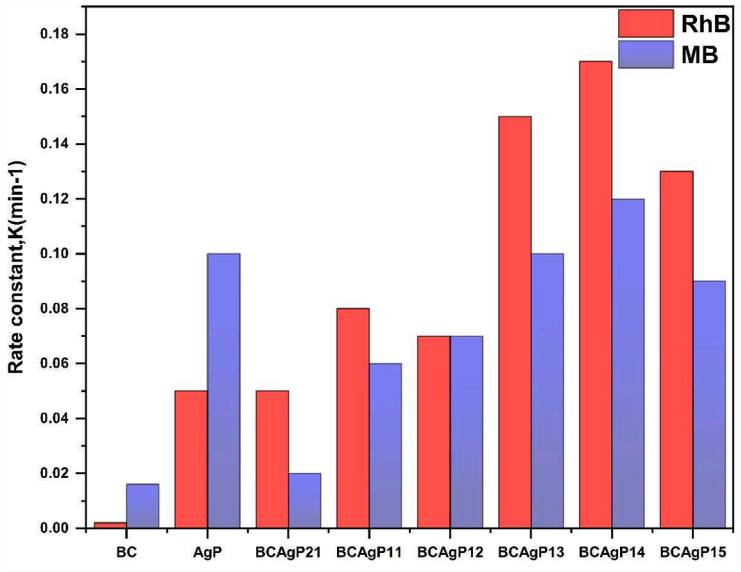

Fig. 9. Rate constants of pure silver phosphate, bacterial cellulose and their composites in 5ppm MB and RhB.

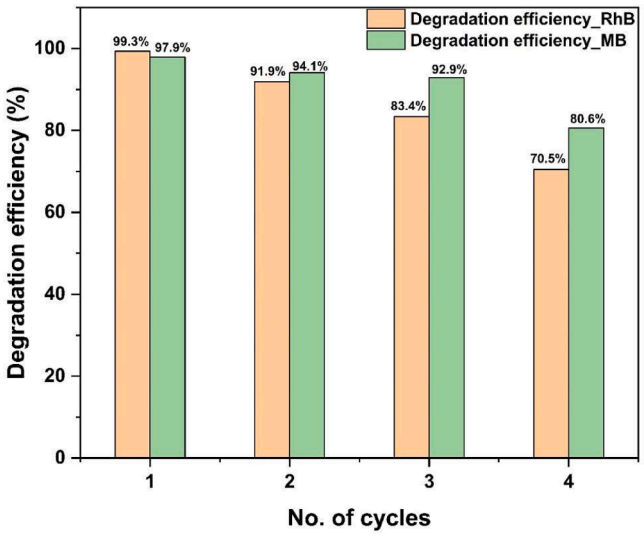

Fig. 10. Reusability test results of BCAgP14 in RhB and MB after 4 runs.

a 300W tungsten lamp. Fig. 7 shows the time v/s C/C_0 plots of pure silver phosphate (AgP), bacterial cellulose (BC), and their composites of different ratios. It is very clear from the plots that the degradation rates of both dyes are more for the BCAgP14 composite than that of AgP and other composites. The rate constants of all the samples were calculated from the plots shown in Fig. 8 using the first-order rate law equation, which connects the reactant concentration at a given time to its beginning concentration. For a first-order reaction, the integral rate law is: $kt = -\ln([C]/[C_0])$, where [C] represents the reactant concentration at time t, $[C_0]$ is the initial reactant concentration, k is the rate constant, and ln is the natural logarithm. A comparison of the rate constants of both dyes in various samples are depicted in Fig. 9. Compared to all other BCAgP nanocomposites, BCAgP14, showed the highest dye degradation rate with a rate constant of 0.173 min^{-1} for RhB and 0.122 min^{-1} for MB, and so it could be considered as the photocatalyst with the best activity. A further increase in Ag3PO4 loading in BC (BCAgP15) reduces the photodegradation efficiency and this might be due to agglomeration and an increase in the size of the Ag3PO4 particle from nano to submicron range (Fig 5j). Also, the rate constants of BCAgP14 and AgP were higher than that of the previously reported works (Lebogang et al., 2019; Liu et al., 2019; Tavker et al., 2020). The rate constant values of all the samples are given in Table 2.

The photo-stability of BCAgP14 (sample having the highest k value)

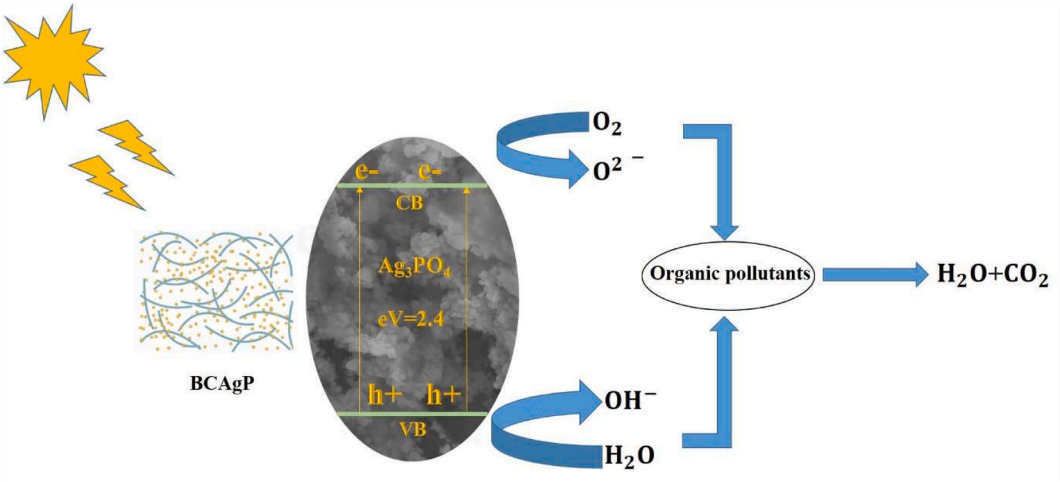

Fig. 11. The schematic representation of the dye degradation mechanism of bacterial cellulose – silver phosphate composites under solar light irradiation.

was evaluated by testing its reusability under the same photocatalytic conditions (0.4 mg in 400 ml 5ppm dye solutions). The sample material was allowed to run for 4 consecutive cycles and it was washed with distilled water and dried after each run. The degradation efficiency of the photocatalyst in RhB and MB has a reduction of 29 % and 17.6 %, respectively. This could be accounted for by the weight loss of the sample after each run (~0.1–0.2 mg) and the adsorption of dyes on the sample surfaces which reduces the active sites for photocatalysis (Tavker et al., 2020). The degradation efficiency of BCAgP14 in 5ppm RhB and MB versus no. of cycles is demonstrated in Fig. 10.

The effect of bacterial cellulose in the photo-stability test is evaluated by performing the recyclability tests of AgP and BCAgP14 in RhB. It was found that BCAgP14 has higher degradation efficiency than pure AgP. This could be attributed to the dye adsorption ability of bacterial cellulose which facilitates the faster degradation of the dyes. The degradation efficiency of BCAgP14 and AgP in RhB after 4 consecutive runs are reported in the supplementary material (Fig. 1).

The pictorial representation of the photocatalysis reaction mechanism of bacterial cellulose-silver phosphate nanocomposite is depicted in Fig. 11. Tavker et al. have reported that when the silver phosphate is irradiated with light, electrons in the material are excited to a higher energy level, creating electron-hole pairs. The electron-hole pairs thus created are separated due to the presence of bacterial cellulose, which traps the photo-excited electrons. The excited electrons can reduce the atmospheric oxygen to O^{2-} radical which could lead to the breakdown of pollutants to carbon dioxide and water, and the holes present in the valance band will react with water molecules and generate hydroxyl radicals (OH*) that are very strong oxidizing agents, which helps in the degradation of organic dyes (Sharma et al., 2015). Also, the adsorption of oxygen onto the cellulose surface will continuously oxidize the dyes, pollutants, etc., and release carbon dioxide and water (Liu et al., 2019). The regenerated electrons can then recombine with the holes trapped in the bulk of the BCAgP nanocomposites to produce more excited electron-hole pairs, which can repeat the photocatalytic process (Tavker et al., 2020). In short, the bacterial cellulose-silver phosphate composites act as a visible light photocatalyst for the degradation of organic pollutants, with bacterial cellulose playing a major role by acting as a support to promote dye adsorption, an electron acceptor and also delaying the recombination rate of electron-hole pairs, which are responsible for the photocatalytic reactions (Chai et al., 2022).

4. Conclusions

Bacterial cellulose - silver phosphate nanocomposites with different BC content were synthesized and characterized. The composite having bacterial cellulose and silver phosphate in the ratio (1:4) was found to be the better visible light active photocatalyst with respect to pure silver phosphate and other composites. It was found that the BCAgP14 has a degradation efficiency of 99.3 % in RhB and 97.1 % in MB within a span of 30 min with a rate constant of 0.173 and 0.122 min^{-1} respectively. The reusability tests results show the photostability of the material even after 4 runs. A reduction of photocatalytic activity was observed after a further increase in silver phosphate content, which might be because it has reached its optimal loading range for maximum photocatalytic efficiency. The incorporation of silver phosphate into bacterial cellulose enhanced the photocatalytic activity since the cellulose act as the acceptor of the photo-excited electrons and hence delays the faster recombination of electron-hole pairs. Bacterial cellulose is an affordable and eco-friendly material that can be considered one of the best natural supports for the production of improved photo-stable catalysts.

Declaration of Competing Interest

The authors declare that they have no known competing financial interests or personal relationships that could have appeared to influence the work reported in this paper.

Data availability

Data will be made available on request.

Supplementary materials

Supplementary material associated with this article can be found, in the online version, at doi:10.1016/j.carpta.2023.100365.

References

Bedia, J., Muelas-Ramos, V., Peñas-Garzón, M., Gómez-Avilés, A., Rodríguez, J. J., & Belver, C. (2019). A review on the synthesis and characterization of metal organic frameworks for photocatalytic water purification. *Catalysts, 9*(1), 52. https://doi.org/10.3390/catal9010052

Chai, Y. D., Pang, Y. L., Lim, S., Chong, W. C., Lai, C. W., & Abdullah, A. Z. (2022). Recent progress on tailoring the biomass-derived cellulose hybrid composite photocatalysts. *Polymers, 14*(23), 5244. https://doi.org/10.3390/polym14235244

Dourado, F., Gama, M., & Rodrigues, A. C. (2017). A review on the toxicology and dietetic role of bacterial cellulose. *Toxicology Reports, 4*, 543–553. https://doi.org/10.1016/j.toxrep.2017.09.005

Fu, J., Yu, J., Jiang, C., & Cheng, B. (2018). G-C3N4-based heterostructured photocatalysts. *Advanced Energy Materials, 8*(3), Article 1701503. https://doi.org/10.1002/aenm.201701503

Fu, L., Zhang, J., & Yang, G. (2013). Present status and applications of bacterial cellulose-based materials for skin tissue repair. *Carbohydrate Polymers, 92*(2), 1432–1442. https://doi.org/10.1016/j.carbpol.2012.10.071

Güzel, M., & Akpınar, Ö. (2019). Production and characterization of bacterial cellulose from citrus peels. *Waste Biomass Valorization, 10*(8), 2165–2175. https://doi.org/10.1007/s12649-018-0241-x

Huang, J., Huang, G., An, C., Xin, X., Chen, X., Zhao, Y., Feng, R., & Xiong, W. (2020). Exploring the use of ceramic disk filter coated with Ag/ZnO nanocomposites as an innovative approach for removing escherichia coli from household drinking water. *Chemosphere, 245*, Article 125545. https://doi.org/10.1016/j.chemosphere.2019.125545

S. J.A. James Martin, D., Liu, G., Moniz, A., Bi, Y., Beale, M., Ye, J., & Tang, J. (2015). Efficient visible driven photocatalyst, silver phosphate: Performance, understanding and perspective *Chemical Society Reviews, 44*(21), 7808–7828. https://doi.org/10.1039/C5CS00380F

Kamel, S. (2004). Preparation and properties of composites made from rice straw and poly(Vinyl Chloride) (PVC). *Polymers for Advanced Technologies, 15*(10), 612–616. https://doi.org/10.1002/pat.514

Krystynowicz, A., Czaja, W., Wiktorowska-Jezierska, A., Gonçalves-Miśkiewicz, M., Turkiewicz, M., & Bielecki, S. (2002). Factors affecting the yield and properties of bacterial cellulose. *Journal of Industrial Microbiology and Biotechnology, 29*(4), 189–195. https://doi.org/10.1038/sj.jim.7000303

Kunjalukkal Padmanabhan, S., Lamanna, L., Friuli, M., Sannino, A., Demitri, C., & Licciulli, A. (2023). Carboxymethylcellulose-based hydrogel obtained from bacterial cellulose. *Molecules, 28*(2), 829. https://doi.org/10.3390/molecules28020829

Lebogang, L., Bosigo, R., Lefatshe, K., & Muiva, C. (2019). Ag_3PO_4/nanocellulose composite for effective sunlight driven photodegradation of organic dyes in wastewater. *Materials Chemistry and Physics, 236*, Article 121756. https://doi.org/10.1016/j.matchemphys.2019.121756

Li, X., Xu, P., Chen, M., Zeng, G., Wang, D., Chen, F., Tang, W., Chen, C., Zhang, C., & Tan, X. (2019). Application of silver phosphate-based photocatalysts: Barriers and solutions. *Chemical Engineering Journal, 366*, 339–357. https://doi.org/10.1016/j.cej.2019.02.083

Lin, S. P., Loira Calvar, I., Catchmark, J. M., Liu, J. R., Demirci, A., & Cheng, K. C. (2013). Biosynthesis, production and applications of bacterial cellulose. *Cellulose, 20*(5), 2191–2219. https://doi.org/10.1007/s10570-013-9994-3

Liu, J., Li, X., Zuo, S., & Yu, Y. (2007). Preparation and photocatalytic activity of silver and TiO_2 nanoparticles/montmorillonite composites. *Applied Clay Science, 37*(3), 275–280. https://doi.org/10.1016/j.clay.2007.01.008

Liu, X., Xu, J., Ni, Z., Wang, R., You, J., & Guo, R. (2019). Adsorption and visible-light-driven photocatalytic properties of Ag_3PO_4/WO_3 composites: A discussion of the mechanism. *Chemical Engineering Journal, 356*, 22–33. https://doi.org/10.1016/j.cej.2018.09.001

Mishra, M., & Chun, D. M. (2015). α-Fe_2O_3 as a photocatalytic material: A review. *Applied Catalysis A: General, 498*, 126–141. https://doi.org/10.1016/j.apcata.2015.03.023

Nash, L. (2008). Purity and danger: Historical reflections on the regulation of environmental pollutants. *Environment and History, 13*(4), 651–658.

Pal, S., Nisi, R., Stoppa, M., & Licciulli, A. (2017). Silver-functionalized bacterial cellulose as antibacterial membrane for wound-healing applications. *ACS Omega, 2*(7), 3632–3639. https://doi.org/10.1021/acsomega.7b00442

Pal, S., Padmanabhan, S. K., Kaitheri, A., Epifani, M., & Licciulli, A. (2023). Efficient solar light photocatalyst made of Ag_3PO_4 Coated TiO_2-SiO_2 Microspheres. *Nanomaterials, 13*(3), 588. https://doi.org/10.3390/nano13030588

Provin, A. P., Cubas, A. L. V., Dutra, A. R., de, A., & Schulte, N. K. (2021). Textile industry and environment: Can the use of bacterial cellulose in the manufacture of biotextiles contribute to the sector? *Clean Technologies and Environmental Policy, 23*(10), 2813–2825. https://doi.org/10.1007/s10098-021-02191-z

Rahmawati, F., Wahyuningsih, S., & Irianti, D. (2014). The photocatalytic activity of SiO_2-TiO_2/graphite and its composite with silver and silver oxide. *Bulletin of Chemical Reaction Engineering & Catalysis, 9*, 45–52. https://doi.org/10.9767/bcrec.9.1.5374.45-52

Rajwade, J. M., Paknikar, K. M., & Kumbhar, J. V. (2015). Applications of bacterial cellulose and its composites in biomedicine. *Applied Microbiology and Biotechnology, 99*(6), 2491–2511. https://doi.org/10.1007/s00253-015-6426-3

Rana, A., Sudhaik, A., Raizada, P., Khan, A. A. P., Van Le, Q., Singh, A., Selvasembian, R., Nadda, A., & Singh, P. (2021). An overview on cellulose-supported semiconductor photocatalysts for water purification. *Nanotechnology for Environmental Engineering, 6*(2), 40. https://doi.org/10.1007/s41204-021-00135-y

Salim, N. E., Nor, N. A. M., Jaafar, J., Ismail, A. F., Qtaishat, M. R., Matsuura, T., Othman, M. H. D., Rahman, M. A., Aziz, F., & Yusof, N. (2019). Effects of hydrophilic surface macromolecule modifier loading on PES/O-g-C_3N_4 hybrid photocatalytic membrane for phenol removal. *Applied Surface Science, 465*, 180–191. https://doi.org/10.1016/j.apsusc.2018.09.161

Sharma, M., Ojha, K., Ganguly, A., & Ganguli, A. K. (2015). Ag_3PO_4 nanoparticle decorated on SiO_2 spheres for efficient visible light photocatalysis. *New Journal of Chemistry, 39*(12), 9242–9248. https://doi.org/10.1039/C5NJ01157D

Shi, Z., Zhang, Y., Phillips, G. O., & Yang, G. (2014). Utilization of bacterial cellulose in food. *Food Hydrocolloids, 35*, 539–545. https://doi.org/10.1016/j.foodhyd.2013.07.012

Srebrenkoska, V., Zhezhova, S., Risteski, S., & Golomeova, S. (2014). *Methods for waste waters treatment in textile industry* (pp. 248–252). International Scientific Conference 21–22.

Szilágyi, I. M., Fórizs, B., Rosseler, O., Szegedi, Á., Németh, P., Király, P., Tárkányi, G., Vajna, B., Varga-Josepovits, K., László, K., Tóth, A. L., Baranyai, P., & Leskelä, M. (2012). WO3 photocatalysts: Influence of structure and composition. *Journal of Catalysis, 294*, 119–127. https://doi.org/10.1016/j.jcat.2012.07.013

U. Tavker, N., Gaur, K., & Sharma, M (2020). Agro-waste extracted cellulose supported silver phosphate nanostructures as a green photocatalyst for improved photodegradation of RhB dye and industrial fertilizer effluents *Nanoscale Advances, 2*(7), 2870–2884. https://doi.org/10.1039/D0NA00181C

Tian, C., Zhang, Q., Wu, A., Jiang, M., Liang, Z., Jiang, B., & Fu, H. (2012). Cost-effective large-scale synthesis of ZnO photocatalyst with excellent performance for dye photodegradation. *Chemical Communications, 48*(23), 2858–2860. https://doi.org/10.1039/C2CC16434E

Yang, J., Liu, D., Song, X., Zhao, Y., Wang, Y., Rao, L., Fu, L., Wang, Z., Yang, X., Li, Y., & Liu, Y. (2022). Recent progress of cellulose-based hydrogel photocatalysts and their applications. *Gels, 8*(5), 270. https://doi.org/10.3390/gels8050270